Available online at www.sciencedirect.com
ScienceDirect
Journal of Magnetic Resonance 188 (2007) 141–150
JMR Journal of Magnetic Resonance
www.elsevier.com/locate/jmr

A least squares quantization table method for direct reconstruction of MR images with non-Cartesian trajectory

Dong Liang, Edmund Y. Lam *, George S.K. Fung

Department of Electrical and Electronic Engineering, The University of Hong Kong, Pokfulam Road, Hong Kong

Received 26 December 2006; revised 27 June 2007
Available online 10 July 2007

Abstract

The direct Fourier transform method is a straightforward solution with high accuracy for reconstructing magnetic resonance (MR) images from nonuniformly sampled *k*-space data, given that the optimal density compensation function is selected and the underlying magnetic field is sufficiently uniform. The computation however is very time-consuming, making it impractical especially for large-size images. In this paper, the least squares quantization table (LSQT) method is proposed to accelerate the direct Fourier transform computation, similar to the recently proposed methods such as using look-up table (LUT) or equal-phase-line (EPL). With LSQT, all the image pixels are first classified into several groups where the Lloyd–Max quantization scheme is used to ensure the minimal classification error. The representative value of each group is stored in a small-size LSQT in advance to reduce the computational load. The pixels in the same group receive the same contribution, which is calculated only once for each group instead of for each pixel, resulting in the reduction of computation because the number of groups is far smaller than the number of pixels. Finally, each image pixel is mapped into the nearest group and its representative value is used to reconstruct the image. The experimental results show that the LSQT method requires far smaller memory size than the LUT method and fewer multiplication operations than the LUT and EPL methods. Moreover, the LSQT method can perform large-size reconstructions that achieve comparable or higher accuracy as compared to the EPL and gridding methods when the appropriate parameters are given. The inherent parallel structure also makes the LSQT method easily adaptable to a multiprocessor system.

PACS: 87.57.Gg; 87.57.-s; 87.61.-c

Keywords: Image reconstruction; Non-Cartesian trajectory; Nonuniform distribution; Lloyd–Max quantization; Least squares quantization table

1. Introduction

In magnetic resonance imaging (MRI), the data are collected in the *k*-space, which is related to the image of the object through a Fourier transform relationship. Many MRI pulse sequences are designed to acquire the *k*-space samples on a Cartesian grid with data acquired on equally spaced grid points. However, this scan pattern can be rather slow in the phase encoding direction [1]. More recently, non-Cartesian scanning in *k*-space, such as using spiral [2,3], rosette [4,5], and stochastic [6] trajectories, has received increasing attention because of a more efficient coverage of the *k*-space, a lower motion sensitivity, and a higher scanning speed. For these scan patterns, image reconstruction can no longer be accomplished directly with a fast Fourier transform (FFT) algorithm. This problem of reconstructing images from a set of nonuniformly sampled data has drawn significant attention in the past few years.

Traditionally, the more commonly used methods are those which benefit from the computational advantage of the FFT, where nonuniformly sampled data are first resampled onto a Cartesian grid, and then the FFT is applied to reconstruct the image. The Kaiser–Bessel gridding method is one of the most widely used gridding algorithms because

* Corresponding author.
E-mail addresses: dliang@eee.hku.hk (D. Liang), elam@eee.hku.hk (E.Y. Lam), skfung@eee.hku.hk (G.S.K. Fung).

1090-7807/$ - see front matter © 2007 Elsevier Inc. All rights reserved.
doi:10.1016/j.jmr.2007.06.013

the Kaiser–Bessel window function was shown to be a desirable choice for the kernel function [7]. There are also methods to choose an optimal parameter combination when using the Kaiser–Bessel window function [8]. The nonuniform FFT (NUFFT) algorithm is another way to solve this problem as it was observed that the gridding algorithm is mathematically equivalent to the type-1 NUFFT problem [9,10]. A related generalized FFT (GFFT) [9] is also equivalent to a gridding algorithm with a Gaussian kernel. Sha et al. proposed a least square NUFFT (LS_NUFFT) method for spiral MRI image reconstruction by minimizing the reconstruction approximation error in the least square sense [10]. The Kaiser–Bessel gridding and NUFFT-based methods have a similar framework, including similar steps of pre-compensation, convolution, FFT, and rescaling. In actual implementation of these techniques, sometimes the reconstructed image is not as accurate as expected, because of the need to carefully select many parameters to appropriate values. Otherwise, they become the major source of degradation in image reconstruction quality.

Alternatives to the above methods also exist. In particular, some researchers aim at a direct mapping from nonuniformly sampled data to grid points [11–15] or the image pixels [16–19]. Rosenfeld and Walle et al. formulated this problem of resampling nonuniformly sampled data onto a Cartesian grid as solving a set of linear equations [11,12]. The advantages of this kind of methods include requiring neither the pre- nor the post-compensation steps, and performing resampling onto a regular grid rather than the oversampled grid. It is, however, sensitive to noise. This is partly resolved by using regularization, estimation theory [14], and truncated singular value decomposition (SVD) [15]. They are iterative reconstruction methods using techniques such as the conjugate gradient descent method. Because the system matrix is large in size and dense, Kadah et al. [18,19] proposed to use a simple transformation to convert the system matrix into a sparse form that leads to much smaller computational and storage efforts.

The direct Fourier transform method is the summation of the inverse Fourier transform of the k-space data weighted by a density compensation function (DCF) [20,21] and has some advantages over the other methods described above. First, it does not require convolution and post-compensation, and therefore reduces the possibilities of introducing reconstruction errors. Second, the reconstructed image can be updated immediately following the most recent information after each individual data point is acquired. This would be important in applications such as MR fluoroscopy. Unfortunately, the high computational demand makes it impractical compared with methods that use the FFT [7,10].

Two algorithms have been proposed to accelerate the direct Fourier transform method recently, with the ultimate objective that this can become a viable alternative to methods mentioned above in selected applications. They are the look-up table (LUT) method [22] and the equal-phase-line (EPL) method [23]. The LUT method saves computations in the Fourier transform method by pre-computing some of them and storing in LUTs. However, this method is only efficient for small-size images due to the huge memory required for storing a LUT. Moreover, though the remaining computation is easy to parallelize, the memory readout to obtain the weights from a table is not, which makes the LUT method time-consuming especially when weights are stored in a large-size table. If the size of the LUT can be reduced so that it is feasible for larger-size images with only a little quality loss, the LUT method can still be appealing. Meanwhile, the EPL method aims to reduce computation by grouping those coefficients associated with the same phase. However, this method does not take into account the actual distribution of phases for each data acquired using non-Cartesian k-space trajectories, and may cause a large quantization error and consequently significant reconstruction quality loss.

In this paper, we propose a least squares quantization table (LSQT) method to accelerate the direct Fourier transform to reconstruct MR images acquired with non-Cartesian trajectory [24]. The basic idea is that because the data in k-space contribute almost equally to various image pixels if they produce roughly the same phase, we can quantize the phase interval of the complex exponential function using the Lloyd–Max quantization technique with the quantized values for reconstruction. In order to reduce the computational load in reconstruction, the representative values of each group can be calculated and stored in a small-size table in advance. In Section 2, we explain the principle of this LSQT method in further details. Implementations and experiments are then described in Section 3. This is followed by some discussions in Section 4 and concluding remarks in Section 5.

2. The least squares quantization table method

The direct Fourier transform method to reconstruct a 2D image I of size $N \times N$ from k-space data s_p with length L is [10,23]:

$$I(x,y) = \sum_{p=1}^{L} s_p d_p \exp\left(j2\pi\left(xu_p + yv_p\right)\right), \tag{1}$$

where $j = \sqrt{-1}, x, y = [-N/2 : N/2 - 1]$ denote an image pixel, and $u_p, v_p = [-1/2 : 1/2]$ is the sampling position in k-space. d_p is the DCF employed to compensate for nonuniform sampling density and is relative to the sampling positions. This is necessary for minimizing the reconstruction error due to uneven sampling of k-space. The contribution of the pth data to the image space is therefore,

$$I_p(x,y) = s_p d_p \exp(j2\pi(xu_p + yv_p)). \tag{2}$$

The final reconstructed image is the sum of the contributions of all data.

It is clear that for a given k-space trajectory, the product of complex exponential function and DCF, i.e.

$T_p(x,y) = d_p \exp(j2\pi(xu_p + yv_p))$, is independent of the k-space data values, and therefore can be pre-computed. Then, Eq. (1) can be written as

$$I(x,y) = \sum_{p=1}^{L} s_p T_p(x,y). \tag{3}$$

Thus, T_ps are essentially the weights that describe how each k-space data point affects the entire image space. In the LUT method, T_ps are pre-calculated and stored in a table with size of $N^2 \times L$, allowing the LUT method to perform the direct Fourier transform reconstruction efficiently. When a data point arrives from the MR scanner, the corresponding weight is loaded, multiplied by the data, and distributed to each pixel of the entire image space. Though T_ps can be calculated and stored in a table off-line to reduce the computation time, if the size of data and image is large, the LUT method is still time-consuming and impractical because it requires huge memory space to load the table. As an example, consider reconstructing a 256×256 image from 10,000 sample points. Assume 2 bytes are needed for each entry in the LUT (since it consists of complex values), we require $256 \times 256 \times 10{,}000 \times 2 \approx 1.22$ GB memory!

It can be seen from Eq. (2) that for a given (u_p, v_p), if two pixels (x_1, y_1) and (x_2, y_2) have the same phase such that $2\pi(x_1u_p + y_1v_p) = 2\pi(x_2u_p + y_2v_p)$, the data s_p has the same contribution to the two pixel locations. Also, we can define $C_p(x,y) = xu_p + yv_p$, and $\langle C_p(x,y)\rangle$ where,

$$\langle C_p(x,y)\rangle = C_p(x,y) - \lfloor C_p(x,y)\rfloor. \tag{4}$$

Note that $\lfloor x \rfloor$ denotes the largest integer smaller than or equal to x. Thus, $0 \leqslant \langle C_p(x,y)\rangle < 1$, and

$$\exp\left(2\pi C_p(x,y)\right) = \exp\left(2\pi\langle C_p(x,y)\rangle\right). \tag{5}$$

Using this notation, it is sufficient to check if certain pixels share the same $\langle C_p\rangle$. If they do, the acquired raw data in k-space will have the same contributions to these pixels.

As such, all the pixels can be classified into different groups based on their $\langle C_p\rangle$ values, where each group is labeled by a representative value. In computing Eq. (2) for image reconstruction, pixels in the same group use the same value for the phase. Because each pixel (x,y) corresponds to a $\langle C_p\rangle$ for a given (u_p, v_p), the problem of classifying pixels to a few groups can be formulated as quantizing their corresponding $\langle C_p\rangle$s into a few bins.

Consequently, Eq. (2) is calculated only once for each group instead of for each pixel in the direct Fourier transform and LUT method. If we have very fine quantization, there will be little loss of accuracy but reduction of computational loads. However, in practice, the reduction is not substantial because if we insist that the elements in a group must be extremely close to the representative value, the number of groups is comparable to the number of pixels [23]. A straightforward alternative is to decrease the number of groups while suffering a loss of reconstruction accuracy. The tradeoff lies in the number of groups, where with fewer groups each one now has a higher tolerance of difference among members in the group.

In the EPL method, each C_p is called one phase line because the pixels that have the same phase lie in a straight line described by equation $xu_p + yv_p = \text{constant}$. Considering the periodic property of the complex exponential function, the EPL method classifies all the pixels into only M phase lines where $M \ll N^2$ by evenly dividing the interval $[0,1)$ of $\langle C_p\rangle$ into M sub-intervals in the main phase band, and each sub-interval represents one phase line with a representative value,

$$E(i) = \frac{i-1}{M}, \quad i = 1, 2, \ldots, M. \tag{6}$$

We can see from Eq. (6) that when the number of groups M is given, all the pixels are classified into the same set of groups for any k-space data, and the representative values of the groups are equidistant. Thus, the EPL method is essentially using a uniform quantization to the phase. This is optimal only when the sample is distributed uniformly. In other words, the EPL method assumes that first, the distributions of $\langle C_p\rangle$ in the interval $[0,1)$ of all k-space data are the same. Second, the distribution of $\langle C_p\rangle$ of any one data (u_p, v_p) is uniform in the interval $[0,1)$. However, for reconstructing image from data sampled by using non-Cartesian k-space trajectories, the distribution of $\langle C_p\rangle$ in the interval $[0,1)$ varies for different k-space data points. Furthermore, in most cases, it is nonuniform for a given (u_p, v_p) (please refer to Appendix A for discussion in more detail), where the distribution may be dense in some sub-regions of $[0,1)$ and sparse in other sub-regions. Therefore, not taking into account the actual distribution of $\langle C_p\rangle$ in the EPL method can lead to larger quantization error and consequently reconstruction quality loss, especially when the quantization bin size is not as fine.

In order to overcome the problems in the LUT and EPL methods, we develop a method that can decrease the size of the table to be feasible for a larger-size image reconstruction compared to the LUT method while suffering a smaller loss of image quality compared to the EPL method. The idea is to use fewer number of groups and decrease the quantization error for $\langle C_p\rangle$. We use the Lloyd–Max least squares quantization algorithm to quantize them into only M bins ($M \ll N^2$), noting that it is optimal even when the sample is distributed nonuniformly [25,26]. Thus, the group boundaries are calculated by quantizing the interval $[0,1)$ into M bins in the least squares sense of quantization error. The representative value of each group is the centroid of the corresponding group, which is the optimal point to give the lowest quality loss. This is given by

$$\mathcal{Q}(i,p) = \frac{1}{N_i} \sum_{d=1}^{N_i} \langle C_p(x_d, y_d)\rangle, \quad i = 1, 2, \cdots M, \tag{7}$$

where N_i is the number of $\langle C_p\rangle$s quantized into the ith bin, and (x_d, y_d) are those pixels classified into this group. Compared to Eq. (6), we can see that firstly, all the pixels are classified into different sets of groups for any k-space data

(u_p, v_p). Secondly, the representative values within one group are not equidistant because it takes into account the actual distribution of $\langle C_p \rangle$ for the particular non-Cartesian trajectory.

Therefore, for the k-space data s with length L, we can pre-compute a least squares quantization table (LSQT) $\mathcal{Q}$ of size $M \times L$. Each column of it stores the M representative values for the corresponding k-space data, and each representative value is a label for a group. This table maps each of the image pixels for a given k-space position to a particular group and representative value. Construction of the table can be accomplished off-line and reused for the same k-space trajectory, as it is independent of the object being imaged. After loading the table, when a new k-space data arrives, its contributions to all the groups can be calculated as

$$b_p(i) = s_p d_p \exp(j2\pi \mathcal{Q}(i,p)), \quad i = 1, 2, \ldots, M. \tag{8}$$

It should be noted that if we define a larger M, the quantization error and reconstruction error will be smaller, but the LSQT size and required memory will be larger. Conversely, a smaller M needs less memory but gives a larger reconstruction error.

To complete the algorithm, we need to define a way to map each pixel to the corresponding group. The way is to search for an entry in the table whose representative value is closest to the current $\langle C_p \rangle$ [26], such as by using a binary-searching algorithm. Moreover, we can exploit symmetry to reduce the searching. Suppose the pixel (x, y) is mapped to the kth group, the contribution of the pth data to the pixel (x, y) will be approximated by $b_p(k)$. Considering the symmetric and periodic properties of $\langle C_p \rangle$, i.e. $\langle C_p(-x,-y) \rangle = \langle -C_p(x,y) \rangle$ and also $\langle C_p(-x,y) \rangle = \langle -C_p(x,-y) \rangle$, pixel $(-x,-y)$ should be classified into the $(M-k)$th group and we can set the corresponding value $b_p(M-k)$ directly. Therefore, only pixels where $x \geqslant 0$ need to undergo mapping [23].

The least squares quantization table-based reconstruction method can be summarized with the following steps:

(1) Load least squares quantization table $\mathcal{Q}$.
(2) Load k-space data s_p and density compensation function d_p, and calculate the product of s_p and d_p.
(3) Calculate the contributions of the pth data to the groups $b_p(i)$, where $i = 1, 2, \ldots, M$.
(4) For each pixel (x, y), calculate $\langle C_p \rangle$ and search for its entry k in $\mathcal{Q}(i,p)$, where $i = 1, 2, \cdots, M$, using binary-searching algorithm.
(5) Distribute $b_p(k)$ to the pixel (x, y) and $b_p(M-k)$ to the pixel $(-x,-y)$.
(6) Go to step (4) for the next pixel with $x \geqslant 0$.
(7) Go to step (2) for the next k-space data.

3. Experimental results

Our experiments were performed with both the Shepp–Logan mathematical phantom [27] and an actual scan spiral data, which contain 13,392 complex data points. We reconstructed an image with size 256×256 from the actual scan data. Three different sizes of the Shepp–Logan phantoms, 64×64, 128×128, and 256×256, are used in our experiments. Spiral trajectory of the actual scan data is used to generate k-space data from these three phantoms following Eq. (16) in [13]. Thus, for the phantom, it has three cases of image reconstruction: $L > N \times N$, $L \approx N \times N$, and $L < N \times N$. We experiment with different number of quantization bins, including $M = 16$, 64, 256, and 1024. The reconstructed 256×256 images using the direct Fourier transform from the actual scan data and phantom data are shown in Fig. 1a and b. We can see the substantial swirling artifacts due to undersampling, as the number of k-space data is only about 20% of the number of image pixels.

3.1. Uniform and Lloyd–Max quantization

To illustrate why the Lloyd–Max quantization scheme has a potential advantage over the uniform quantization used in the EPL method, we first plot the probability density functions of $\langle C_p \rangle$ for some sample points. The cases for $p = 745$, i.e. $(u_p = 5.439 \times 10^{-6}, v_p = 1.980 \times 10^{-6})$, $p = 1900$, i.e. $(u_p = -3.572 \times 10^{-2}, v_p = 1.768 \times 10^{-1})$, and $p = 5972$, i.e. $(u_p = -8.824 \times 10^{-3}, v_p = -5.998 \times 10^{-3})$, are shown in Fig. 2a–c, respectively. They are all nonuniformly distributed, although to different extent. From (a), we can see that the distribution of $\langle C_{745} \rangle$ is highly nonuniform, because all the $\langle C_{745} \rangle$s are concentrated in two small regions, namely $0 \leqslant \langle C_{745} \rangle \leqslant 0.00094969$ and $0.99905 \leqslant \langle C_{745} \rangle \leqslant 0.99999$. The probability density is zero in between these two regions. In (b), the distribution of $\langle C_{1900} \rangle$ is closer to uniform, as the probability density function is almost a constant in the entire interval $[0, 1)$. In between these two more extreme cases, the nonuniform distribution of $\langle C_{5972} \rangle$, shown in (c), is more common. In this case, the probability density function is a constant in some sub-intervals, and a linear function in some other sub-intervals, in agreement with the discussion in Appendix A. Additionally, it should be noted that the distribution of $\langle C_p \rangle$ is different for different k-space sample point.

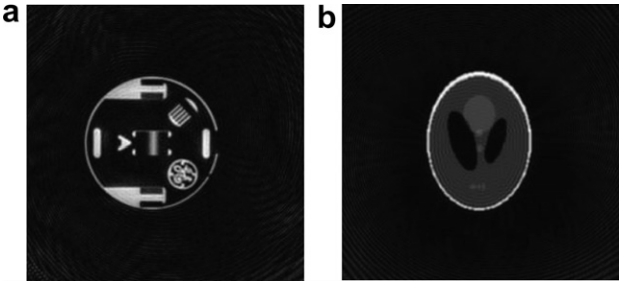

Fig. 1. (a and b) The reconstructed images obtained using the direct Fourier transform method from actual scan data and phantom data with size 256×256, respectively.

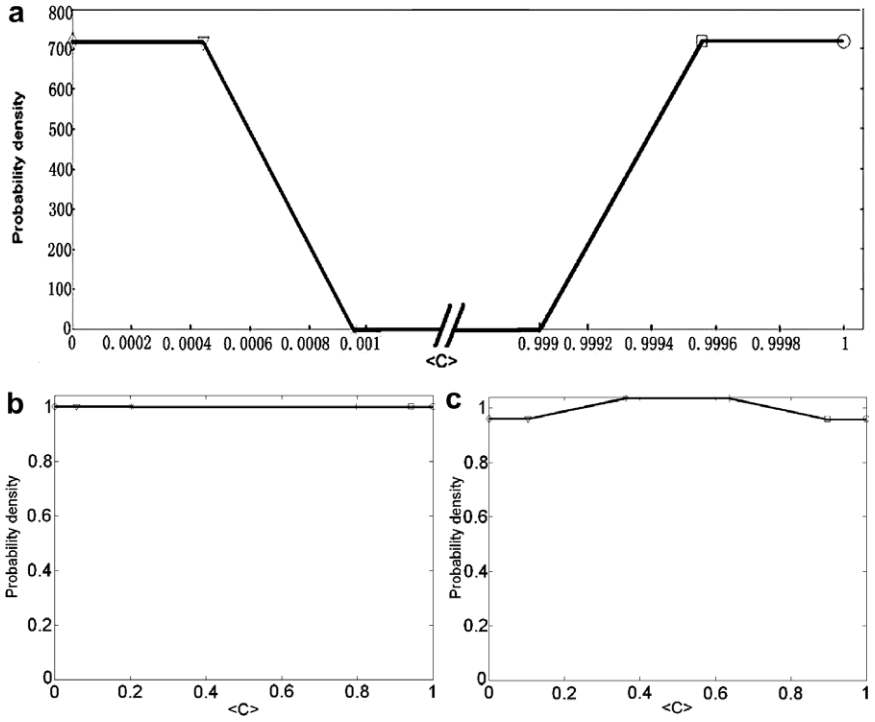

Fig. 2. (a–c) The probability density function of $\langle C_{745}\rangle$, $\langle C_{1900}\rangle$, and $\langle C_{5972}\rangle$, respectively.

Equipped with this knowledge, we further illustrate the difference between uniform quantization and Lloyd–Max least squares quantization algorithms using an actual scan data. Consider the more extreme case of $p = 745$ discussed above. Table 1 gives the representative values of 16 groups of $\langle C_{745}\rangle$ obtained using two different quantization algorithms. This table can be regarded as a codebook. In accordance with Eq. (6), the representative values of the uniform quantization algorithm are evenly distributed in the entire interval $[0, 1)$, while those of the least squares quantization algorithm are distributed in the two regions where the original $\langle C_{745}\rangle$s locate. This is because the least squares quantization algorithm takes into account the actual distribution of the original signal. It should be noted that considering the periodic property of the complex exponential function when performing quantization operation, the values that are smaller than the first representative value or larger than the last representative value and closer to 1 will be quantized to the first bin.

Table 1
The representative values of 16 groups of $\langle C_{745}\rangle$ using uniform quantization and Lloyd–Max quantization

i	Uniform	Least squares	i	Uniform	Least squares
1	0	0.0000466	9	0.5	0.99922
2	0.0625	0.0001399	10	0.5625	0.99937
3	0.125	0.0002333	11	0.625	0.99948
4	0.1875	0.0003270	12	0.6875	0.99958
5	0.25	0.0004202	13	0.75	0.99967
6	0.3175	0.0005173	14	0.8125	0.99977
7	0.375	0.0006313	15	0.875	0.99986
8	0.4375	0.0007843	16	0.9375	0.99995

Consider an example where the original value of one $\langle C_{745}\rangle$ is 0.00094969. It is quantized to the first bin with a representative value of 0 in the uniform quantization algorithm. The quantization error is then 0.00094969. The corresponding pixel is classified into the first group with $b_{745}(1) = s_{745}d_{745}$ according to Eq. (8). On the other hand, in the least squares quantization algorithm, this $\langle C_{745}\rangle$ is quantized to the eighth bin with the representative value of 0.0007843. The quantization error in this case is only $|0.00094969 - 0.00078430| = 0.00016539$. The corresponding pixel is classified into the eighth group with $b_{745}(8) = s_{745}d_{745}\exp(j2\pi \times 0.0007843)$. Comparing the two, the quantized $\langle C_{745}\rangle$ of least squares quantization algorithm is closer to the original $\langle C_{745}\rangle$, which means that the least squares quantization algorithm gives a more accurate quantization result, which will lead to better image reconstruction quality. Furthermore, in uniform quantization, all the 256×256 pixels for the 745th data are classified into one group and are receiving the same contribution, while they can be classified into as many as 16 groups using least squares quantization algorithm. Thus, the approximation of the contribution using the least squares quantization algorithm is more accurate than that using the uniform quantization algorithm.

We can measure the l_1 norm of the quantization error using the formula:

$$E = \sum_{d=1}^{N\times N}\sum_{p=1}^{L}\left|\langle C_p(x_d, y_d)\rangle - \langle C_p(x_d, y_d)\rangle^{Q}\right| \tag{9}$$

where $\langle C_p(x_d, y_d)\rangle^{Q}$ denotes $\langle C_p(x_d, y_d)\rangle$ after quantization. This measurement can help us compare the efficacy of

uniform quantization and least squares quantization. In our experiments, for $M = 16$, 64, 256, and 1024, the quantization errors E of $256^2 \times 13392$ fractional parts for least squares quantization algorithm are only 31.98%, 29.11%, 25.01%, and 21.28%, respectively, of that for uniform quantization, again showing the advantage of using the former.

3.2. Reconstruction accuracy

The "ideal" images obtained with the direct Fourier transform method were used as standards to compare the LSQT method with the EPL and gridding methods. In our work, an oversampling ratio of 1.5 and a kernel width of 4 were chosen for gridding, and the shape parameter and optimal sampled kernel were calculated using the method proposed by Beatty et al. [8]. All the algorithms were implemented in MATLAB and C++ on a personal computer (Intel Pentium 4 2.4 GHz processor with 512 MB of RAM). The absolute difference image, normalized root mean square (nRMS) error and maximum absolute difference (MAD) between the ideal and reconstructed images were used to evaluate the reconstruction performance. The nRMS and MAD are defined as [16]:

$$\mathrm{nRMS} = \sqrt{\frac{\sum_{x=1}^{N}\sum_{y=1}^{N}(I(x,y) - I_{\mathrm{r}}(x,y))^2}{\sum_{x=1}^{N}\sum_{y=1}^{N}(I(x,y))^2}} \tag{10}$$

and

$$\mathrm{MAD} = \frac{\max_{x,y}|I(x,y) - I_{\mathrm{r}}(x,y)|}{255}, \tag{11}$$

where $I(x,y)$ and $I_{\mathrm{r}}(x,y)$ are the ideal and reconstructed images, respectively, scaled to 8 bits unsigned integers. It is also possible to use either floating point or 16-bit integers which are also common for medical images.

Fig. 3 compares the absolute difference images of reconstruction with actual scan data using the EPL and LSQT methods, where the first row is for the EPL method and the second row is for the LSQT method. All difference images were amplified 100 times and any value in the amplified difference images greater than 255 will be displayed as white to improve contrast visibility. In this figure, $M = 16$ for (a) and (e), 64 for (b) and (f), 256 for (c) and (g), and 1024 for (d) and (h). In all four cases, when the EPL method and LSQT method share the same M, the latter is seen to distribute the error more evenly and have a lower peak gray level than the former. For both methods, the number of pixels having large difference between the ideal and reconstructed images decreases with increasing M. This underscores the fact that the reconstruction error can be reduced with a larger M. Similar conclusions can also be drawn from Fig. 4, which shows the comparisons using the Shepp–Logan phantom. The trends of the amplified difference images for the two methods and the four values of M also confirm that increasing M can reduce the reconstruction error, and LSQT generally outperforms EPL significantly for the same value of M.

Next, we compare the LSQT method and the gridding method, using the parameters mentioned earlier in this section. Fig. 5a and b shows the difference images magnified 1000 times obtained by the gridding method with actual scan data and Shepp–Logan phantom, respectively. We can see that the reconstruction errors mainly lie along the outer regions of the image. In comparison, Fig. 5c and d shows the difference images magnified 1000 times obtained by the LSQT method (with $M = 1024$), again for the scan data and phantom. Here, the reconstruction errors are seen to distribute more evenly over the image, resulting in a lower maximum error.

In addition to visual comparisons, we also measure the reconstruction quality using nRMS and MAD. Table 2 shows the nRMS computed with the actual scan data using the different methods when we vary the number of groups. Table 3 is a similar table with MAD instead. Using either metric, we can see that the LSQT method has similar reconstruction quality when $M = 1024$ compared with gridding using the parameters mentioned above, and is superior to the EPL method when two methods take the same value for M for all four cases. Moreover, comparing

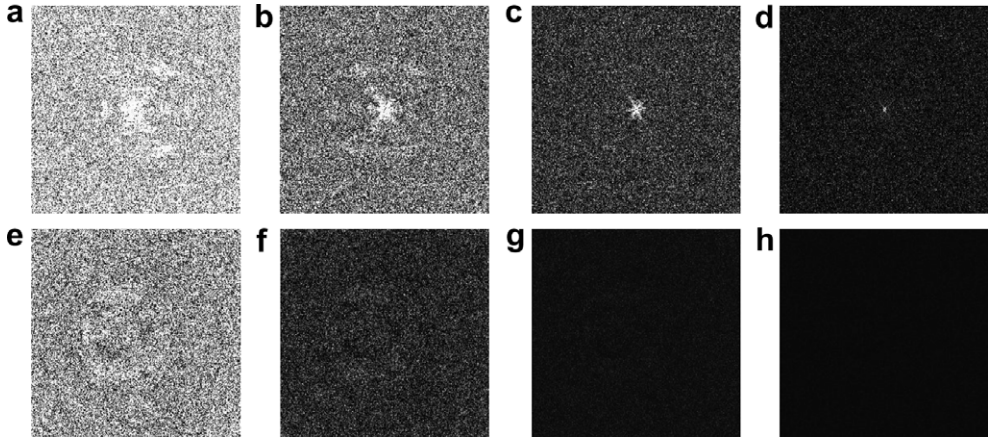

Fig. 3. The absolute difference images for reconstruction with actual scan data. The first row (a–d), where M equals to 16, 64, 256, and 1024, respectively, is for the EPL method, and the second row (e–h) is for the LSQT method. All difference images were amplified 100 times.

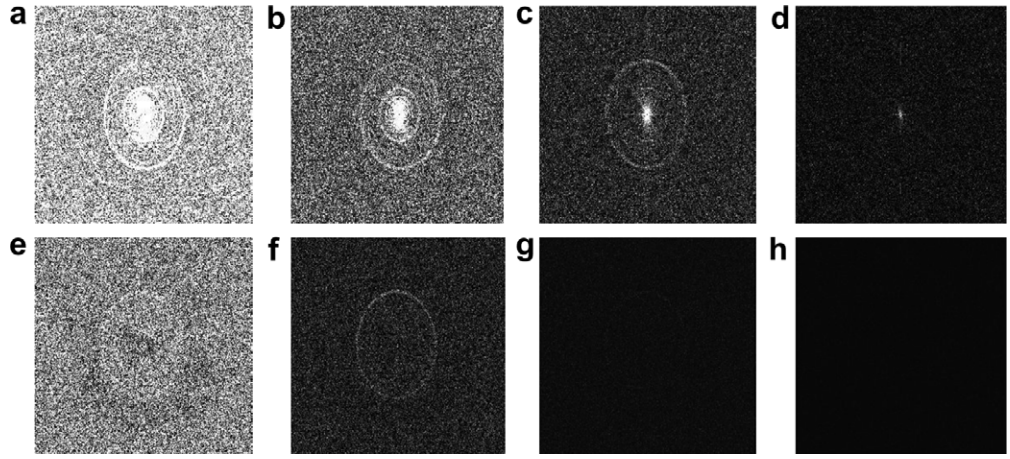

Fig. 4. The absolute difference images for reconstruction with Shepp–Logan phantom. The first row (a–d), where M equals to 16, 64, 256, and 1024, respectively, is for the EPL method, and the second row (e–h) is for the LSQT method. All difference images were amplified 100 times.

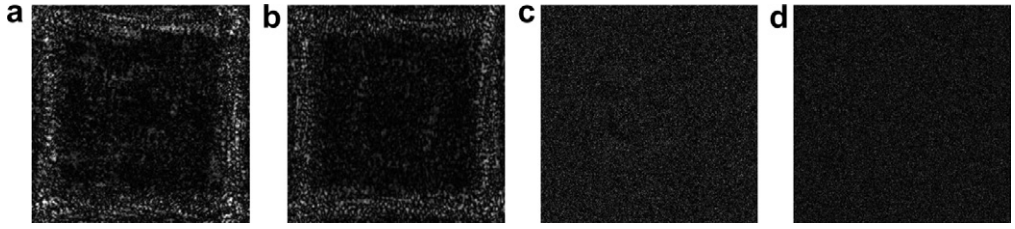

Fig. 5. (a and b) The difference images amplified 1000 times obtained by using the gridding method with actual scan data and Shepp–Logan phantom, respectively. (c and d) The difference images amplified 1000 times obtained by using the LSQT method with $M = 1024$ from actual scan data and Shepp–Logan phantom, respectively.

Table 2
The nRMS of the various methods against the number of groups, M, using actual scan data

	$M = 16$	$M = 64$	$M = 256$	$M = 1024$
LSQT	0.06642	0.01671	0.00402	0.00094
EPL	0.11307	0.04672	0.02174	0.01061
Gridding	0.00126			

the columns in the two tables, when we increase M by a factor of 4, both the nRMS and MAD decrease to less than a quarter of the previous case. This trend is also true when we experiment with the Shepp–Logan phantom. As discussed earlier, increasing M requires a larger memory requirement. Because each element of a LSQT is a real fractional part and can be represented as a 4 bytes float type without a noticeable loss in accuracy, the required memory for loading a table is roughly $4ML$ bytes, i.e. 0.82, 3.27, 13.08, and 52.31 MB for $M = 16$, 64, 256, and 1024, respectively. This is compared to 6696 MB for the LUT method because each element of a LUT is a complex fractional part and requires twice the space to store compared to LSQT. It is clear that reconstructing an image with such a size using the LUT method is impractical. Put another way, an 8 MB of memory that is required for reconstructing a 32×32 image from 1024 data using LUT in [22] is sufficient to reconstruct a 256×256 image from 13,392 spiral trajectory data with $M = 128$ in our experiments.

Table 3
The MAD of the various methods against the number of groups, M, using actual scan data

	$M = 16$	$M = 64$	$M = 256$	$M = 1024$
LSQT	0.05323	0.01183	0.00291	0.00067
EPL	0.14144	0.10161	0.05120	0.01369
Gridding	0.00134			

3.3. The reusability of LSQT

As we described above, the LSQT constructed for a given trajectory can be reused for reconstructing different images with the same size. This is because constructing LSQT is only dependent on the k-space sampling positions and image pixels positions. Moreover, another advantage of LSQT method is that the LSQT constructed in the case of $L < N \times N$ can be reused in the case of $L \approx N \times N$ and $L > N \times N$ where L is fixed. Fig. 6a and b shows the nRMS and MAD of LSQT method against the number of groups for reconstructing different size of phantoms with different LSQTs. Here, LSQT256 N64 and LSQT256 N128 mean reconstructing a 64×64 or 128×128 phantom but with a LSQT constructed for reconstructing a 256×256 phantom from the same k-space data. LSQT64 N64 and LSQT128

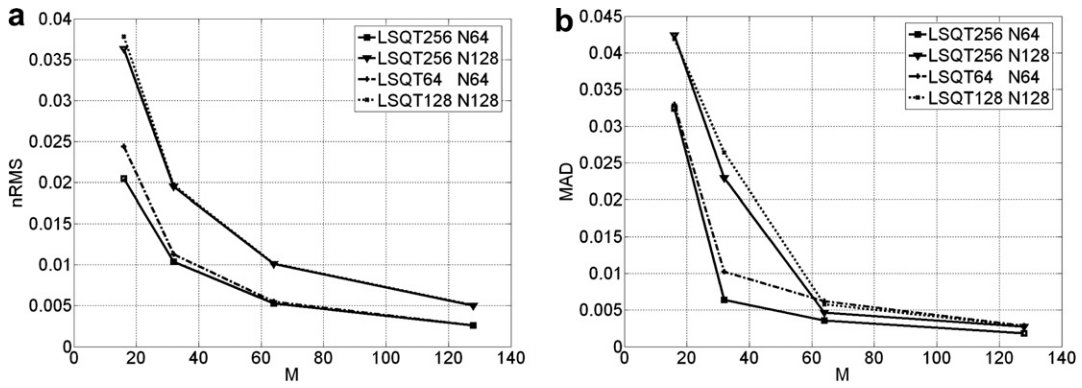

Fig. 6. (a and b) The nRMS and MAD of LSQT method against the number of groups for reconstructing different size of phantoms with different LSQTs.

N128 refer to the reconstruction of a 64×64 or 128×128 phantom with their own LSQTs. It can be seen that reconstructing 64×64 and 128×128 phantoms with LSQT256 performs better than with their own LSQTs using both nRMS and MAD as the metric. The reason is that each element of LSQT256 is obtained from 256×256 $\langle C_p \rangle$s in the interval $[0, 1)$ while each element of LSQT64 and LSQT128 is obtained from 64×64 or 128×128 $\langle C_p \rangle$s in the interval $[0, 1)$. Obviously, the representative values stored in LSQT256 are more precise than those stored in LSQT64 and LSQT128 when $\langle C_p \rangle$s have similar distribution. This advantage means the LSQT method can be reused not only for reconstructing different images with the same size, but for reconstructing different images of reduced size.

The selection of the number of groups affects the quantization precision and the size of LSQT, and hence the reconstruction accuracy and required memory. Therefore, the selection of M is flexible in trading-off required memory against reconstruction error in our method. For example, if a high accuracy is desired, it is easy to implement by increasing the number of groups. It can be suggested that when $L > N \times N$, M can take a small value while when $L < N \times N$, M should take a larger value to retain a substantial reduction in reconstruction error.

3.4. Computational complexity

When mapping the data s_p to image I in Eq. (1), it requires about $\frac{5}{2}N^2L$ complex multiplications for the direct Fourier transform method, with one real multiplication counted as 1/4 complex multiplication [23]. For the LUT method, there are N^2L complex multiplications. The EPL method requires $L\left(\frac{1}{2} + \frac{3}{2}M + \frac{3}{8}N^2\right)$ and the LSQT method requires $L\left(\frac{1}{2} + \frac{3}{2}M + \frac{1}{4}N^2\right)$ complex multiplications. When $M \ll N^2$, the required operations of complex multiplication in the EPL and LSQT methods are approximately $\frac{3}{8}N^2L$ and $\frac{1}{4}N^2L$, respectively, i.e. about 15 and 10% compared with direct Fourier transform. It should also be pointed out that the EPL and LSQT methods have computational complexity of $O(N^2L)$ because we need to calculate C_p for each image pixel and each sampling position. The gridding method however only requires $\frac{1}{2}L + 36N^2 + \frac{9}{4}N^2\log_2\left(\frac{3}{2}N\right)$ complex multiplications using FFT [23].

When realizing these methods, the total reconstruction time includes three parts: calculating contribution for each data (as in Eq. (8)), computing $\langle C_p \rangle$ for each data and image pixel (as in Eq. (4)), and mapping pixels to the corresponding groups (which involves no multiplication in this part). In our implementation, the direct Fourier transform takes about 460 s, gridding method time is about 0.3 s and the EPL and LSQT need about 151 and 211 s, respectively. Most time is spent in mapping operations in the EPL and LSQT methods. We did not compare the time for the LUT method because the large-size table cannot be loaded into the memory. In [22], where this method was proposed, the reconstruction time for larger-size images were estimated by extrapolation.

4. Discussion

LSQT has a fairly straightforward implementation. This is somewhat simpler than gridding, which requires optimization of a few parameters. For example, the user needs to choose certain specific parameters for reconstruction, such as the kernel width or oversampling ratio [7,8,11]. To find the optimal presampled kernel also requires solving a second-order cone program (SOCP) [8]. Instead, in LSQT a single parameter can be used for quality measure and computational load control. The tradeoff for a better image quality is a larger memory. Therefore, the LSQT method can be customized for the particular application by selecting a predetermined number of groups that corresponds to the desired required memory, or for some applications where image quality is a lot more important than reconstruction time. Additionally, in some applications where the most recent information carried by each individual data point needs to be presented, the LSQT method can update the reconstructed image immediately after each individual data point is acquired while the gridding method has to perform an FFT for each reconstruction update.

At present, the LSQT method is more time-consuming than the Kaiser–Bessel gridding method. However, there are ways to improve the speed of LSQT with a sufficient

number of processing units. The reason is that table-based methods are highly amenable to parallelization. Some researchers have explored multiprocessor and dedicated hardware systems for image reconstruction from nonuniformly sampled data [28–30]. For the LSQT method, $b_p(i)$s only need to be calculated M times for each data. Therefore, it may be accelerated by using a more efficient searching algorithm and a multiprocessor system.

Another point to note is that inhomogeneity effect has not been considered in this paper. In the presence of field inhomogeneity, the MRI signal and the image do not have a Fourier transform relationship. It involves a complex exponential function with irregular sampling in both domains, and will cause more severe blurring and other artifacts for non-Cartesian acquisitions than for Cartesian acquisitions [16,31]. The LSQT method could be a potential solution to this problem by integrating the inhomogeneity term into the phase, while the quantization would need to be recalculated for each slice. Additionally, if one is willing to tolerate memory requirements on the order of the LSQT method, the mappings can be pre-calculated and the number of multiplications becomes O(ML), representing a significant advantage in reducing the computational loads.

5. Conclusion

In this paper, a LSQT-based method is proposed to improve the direct reconstruction from nonuniformly sampled MRI data. It requires far less memory than the LUT method when reconstructing images of the same size. Compared with the gridding and EPL methods, the LSQT method can provide reconstructions that are comparable to or more accurate when the appropriate parameter is chosen. In addition, it requires fewer complex multiplications than the LUT and EPL methods. These advantages make this a potential alternative to other image reconstruction methods for nonuniform MRI data.

Acknowledgments

The authors thank Brian Hargreaves for making available the actual spiral scan data at http://www-mrsrl.stanford.edu/~brian/gridding/, Philip J. Beatty for providing the gridding reconstruction program, Jeffrey A. Fessler for helpful comments, and the anonymous journal referees whose input improved this work. This work was supported in part by the University Research Committee of the University of Hong Kong under Projects 10207440 and 10205870.

Appendix A

Here, we discuss the distribution of $\langle C_p\rangle = \langle xu_p + yv_p\rangle$ for a given (u_p, v_p), where $-\frac{1}{2} \leqslant u_p \leqslant \frac{1}{2}$ and $-\frac{1}{2} \leqslant v_p \leqslant \frac{1}{2}$. The distributions of x and y are uniform in the interval $[-\frac{N}{2}, \frac{N}{2}]$. Therefore, C_p is a weighted sum of two uniform distributions with zero mean. Consequently, the probability density function of C_p is trapezoidal in shape [32]. Without loss of generality, let us assume $|u_p| > |v_p|$, and let

$$g = \frac{N}{2}\left(|u_p| + |v_p|\right) \qquad \text{and} \qquad h = \frac{N}{2}\left(|u_p| - |v_p|\right), \tag{12}$$

where it is clear that $g \geqslant h$. Then, the probability density function of C_p is

$$p(C_p) = \begin{cases} \frac{g+C_p}{g^2-h^2} & : \quad -g \leqslant C_p < -h \\ \frac{1}{g+h} & : \quad -h \leqslant C_p < h \\ \frac{g-C_p}{g^2-h^2} & : \quad h \leqslant C_p < g \\ 0 & : \quad \text{otherwise.} \end{cases} \tag{13}$$

This is shown in Fig. 7.

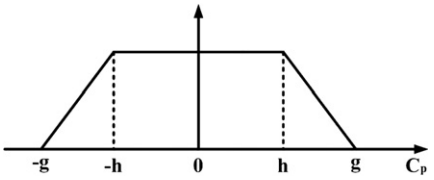

Fig. 7. The trapezoidal distributions of C_p.

We can form the probability density function of $p(\langle C_p\rangle)$ from the equation above by "folding" all the regions to $[0, 1)$. While we can form analytical expressions through tedious calculations, it is sufficient for our purpose here to see that in general, $p(\langle C_p\rangle)$ will not be uniformly distributed. There are exceptions, such as when $g = h$, which implies that $|v_p| = 0$. However, in a general setting, the two ends of the trapezoidal do not overlap exactly during folding, and the resulting nonuniform distribution necessitates the use of Lloyd–Max least squares quantization rather than uniform quantization.

References

[1] Z.P. Liang, P.C. Lauterbur, Principles of Magnetic Resonance Imaging: A Signal Processing Perspective, IEEE Press, New York, 2000.
[2] D.C. Noll, Methodologic considerations for spiral k-space functional MRI, Int. J. Imaging Syst. Technol. 6 (1995) 175–183.
[3] J.H. Duyn, Y.H. Yang, Fast spiral magnetic resonance imaging with trapezoidal gradients, J. Magn. Reson. 128 (1997) 130–134.
[4] D.C. Noll, Multi-shot rosette trajectories for spectrally selective MR imaging, IEEE Trans. Med. Imaging 16 (1997) 372–377.
[5] D.C. Noll, S. Peltier, F. Boada, Simultaneous multislice acquisition using rosette trajectories (SMART): a new imaging method for functional MRI, Magn. Reson. Med. 39 (1998) 709–716.
[6] K. Scheffler, J. Hennig, Frequency resolved single-shot MR imaging using stochastic k-space trajectories, Magn. Reson. Med. 35 (1996) 569–576.
[7] J.I. Jackson, C.H. Meyer, D.G. Nishimura, A. Macovski, Selection of a convolution function for Fourier inversion using gridding, IEEE Trans. Med. Imaging 10 (1991) 473–478.
[8] P.J. Beatty, D.G. Nishimura, J.M. Pauly, Rapid gridding reconstruction with a minimal oversampling ratio, IEEE Trans. Med. Imaging 24 (2005) 799–808.
[9] G. Sarty, R. Bennett, R. Cox, Direct reconstruction of non-Cartesian k-space data using a nonuniform fast Fourier transform, Magn. Reson. Med. 45 (2001) 908–915.

[10] L.W. Sha, H. Guo, A.W. Song, An improved gridding method for spiral MRI using nonuniform fast Fourier transform, J. Magn. Reson. 162 (2003) 250–258.
[11] D. Rosenfeld, An optimal and efficient new gridding algorithm using singular value decomposition, Magn. Reson. Med. 40 (1998) 14–23.
[12] R.V. de Walle, H.H. Barrett, K.J. Myers, M.I. Altbach, B. Desplanques, A.F. Gmitro, J. Cornelis, I. Lemahieu, Reconstruction of MR images from data acquired on a general nonregular grid by pseudoinverse calculation, IEEE Trans. Med. Imaging 19 (2000) 1160–1167.
[13] H. Moriguchi, M. Wendt, J.L. Duerk, Applying the uniform resampling (URS) algorithm to a lissajous trajectory: fast image reconstruction with optimal gridding, Magn. Reson. Med. 44 (2000) 766–781.
[14] D. Rosenfeld, New approach to gridding using regularization and estimation theory, Magn. Reson. Med. 48 (2002) 193–202.
[15] H. Moriguchi, M. Wendt, J.L. Duerk, Modified block uniform resampling (BURS) algorithm using truncated singular value decomposition: fast accurate gridding with noise and artifact reduction, Magn. Reson. Med. 46 (2001) 1189–1201.
[16] B.P. Sutton, D.C. Noll, J.A. Fessler, Fast, iterative image reconstruction for MRI in the presence of field inhomogeneities, IEEE Trans. Med. Imaging 22 (2003) 178–188.
[17] B. Desplanques, J. Cornelis, E. Achten, R.V. de Walle, I. Lemahieu, Iterative reconstruction of magnetic resonance images from arbitrary samples in *k*-space, IEEE Trans. Med. Imaging 49 (2002) 2268–2273.
[18] Y.M. Kadah, New solution to the gridding problem, in: Proceedings of SPIE Medical Imaging 2002: Image Processing, vol. 4684, 2002, pp. 1–9.
[19] Y.M. Kadah, A.S. Fahmy, R.E. Gabr, K. Heberlein, X.P. Hu, Progressive magnetic resonance image reconstruction based on iterative solution of a sparse linear system, Int. J. Biomed. Imaging 2006 (2006) 1–9.
[20] A. Maeda, K. Sano, T. Yokoyama, Reconstruction by weighted correlation for MRI with time-varying gradients, IEEE Trans. Med. Imaging 7 (1988) 26–31.
[21] G. Sarty, The natural *k*-plane coordinate reconstruction method for magnetic resonance imaging: mathematical foundations, Int. J. Imaging Syst. Technol. 8 (1997) 519–528.
[22] B. Dale, M. Wendt, J.L. Duerk, A rapid look-up table method for reconstructing MR images from arbitrary *k*-space trajectories, IEEE Trans. Med. Imaging 20 (2001) 207–216.
[23] Y.X. Qian, J.R. Lin, D.Q. Jin, Direct reconstruction of MR images from data acquired on a non-Cartesian grid using an equal-phase-line algorithm, Magn. Reson. Med. 47 (2002) 1228–1233.
[24] D. Liang, E.Y. Lam, G.S.K. Fung, Direct reconstruction of spiral MRI using least squares quantization table, in: IEEE International Symposium on Biomedical Imaging: From Nano to Macro, 2007, pp. 105–108.
[25] S. Lloyd, Least squares quantization in PCM, IEEE Trans. Inf. Theory IT-28 (1982) 129–137.
[26] A. Gersho, R.M. Gray, Vector Quantization and Signal Compression, Kluwer Academic Publishers, Boston, 1992.
[27] L.A. Shepp, B.F. Logan, The Fourier reconstruction of a head section, IEEE Trans. Nucl. Sci. NS-21 (1974) 21–43.
[28] H. Eggers, R. Proska, Multiprocessor system for real-time convolution interpolation reconstruction, in: Proc. ISMRM 7th Annu. Meet., vol. 1, 1999, p. 95.
[29] S. Thomas, T. Chang, P. Speierb, R. Westermannc, MR image reconstruction using the GPU, in: Proceedings of SPIE Medical Imaging 2006: Physics of Medical Imaging, vol. 6142, 61423T, 2006, pp. 1–12.
[30] A.B. Kerr, J.M. Pauly, B.S. Hu, K.C. Li, C.J. Hardy, C.H. Meyer, A. Macovski, D.G. Nishimura, Real-time interactive MRI on a conventional scanner, Magn. Reson. Med. 38 (1997) 355–367.
[31] H. Eggers, T. Knopp, D. Potts, Field inhomogeneity correction based on gridding reconstruction for magnetic resonance imaging, IEEE Trans. Med. Imaging 26 (2007) 374–384.
[32] A. Papoulis, S. Pillai, Probabilty, Random Variables and Stochastic Processes, fourth ed., McGraw-Hill, New York, 2002.